Global Assessment of Benthic Nepheloid Layers and Linkage with Upper Ocean Dynamics

*Wilford D. Gardner[a]
a Texas A&M University
College Station, TX 77843
USA
wgardner@ocean.tamu.edu

Mary Jo Richardson[b]
b Department of Oceanography
Texas A&M University
College Station, TX 77843
USA
mrichardson@ocean.tamu.edu

Alexey V. Mishonov[c]
c Cooperative Institute for Climate and Satellites (CICS), University of Maryland
National Centers for Environmental Information (NCEI), NOAA affiliate
Silver Spring, MD 20910
USA
alexey.mishonov@noaa.gov

*Corresponding author: wgardner@ocean.tamu.edu

Abstract

Global maps of the maximum bottom concentration, thickness, and integrated particle mass in benthic nepheloid layers are published here to support collaborations to understand deep ocean sediment dynamics, linkage with upper ocean dynamics, and assessing the potential for scavenging of adsorption-prone elements near the deep ocean seafloor. Mapping the intensity of benthic particle concentrations from natural oceanic processes also provides a baseline that will aid in quantifying the industrial impact of current and future deep-sea mining. Benthic nepheloid layers have been mapped using 6,392 full-depth profiles made during 64 cruises using our transmissometers mounted on CTDs in multiple national/international programs including WOCE, SAVE, JGOFS, CLIVAR-Repeat Hydrography, and GO-SHIP during the last four decades. Intense benthic nepheloid layers are found in areas where eddy kinetic energy in overlying waters, mean kinetic energy 50 meters above bottom (mab), and energy dissipation in the bottom boundary layer are near the highest values in the ocean. Areas of intense benthic nepheloid layers include the Western North Atlantic, Argentine Basin in the South Atlantic, parts of the Southern Ocean and areas around South Africa. Benthic nepheloid layers are weak or absent in most of the Pacific, Indian, and Atlantic basins away from continental margins. High surface eddy kinetic energy is associated with the Kuroshio Current east of Japan. Data south of the Kuroshio show weak nepheloid layers, but no transmissometer data exist beneath the Kuroshio, a deficiency that should be remedied to increase understanding of eddy dynamics in un-sampled and under-sampled oceanic areas.

Keywords

Benthic nepheloid layers
Eddy kinetic energy
Particulate matter
Benthic storms
Erosion
Resuspension

Highlights

Benthic nepheloid layers are most intense beneath areas of high eddy kinetic energy
Deep western boundary currents are too weak to generate intense nepheloid layers
Benthic storms erode the seafloor and maintain the benthic nepheloid layer
Benthic nepheloid layers are weak to non-existent in areas of low eddy kinetic energy
High benthic kinetic energy and energy dissipation match strong nepheloid layers

1. Introduction

Optical instruments have been used for many decades to measure turbidity in bodies of water to estimate particle abundance and distribution (Biscaye and Eittreim, 1977; Gardner et al., 2017; Jerlov, 1953). It has long been known that particle concentrations are elevated in the euphotic zone resulting mostly from primary production of phytoplankton (up to 100's to 1000's µg l^{-1}), or river discharge into lakes or oceans (µg's to g's/l). Particles are not long-term conservative components in water because they can sink or rise depending on their density, thus moving across isopycnals, as well as being advected or subducted with the surrounding water. Consequently, particles can transport mass downward even through a stratified water column. Some dissolved or colloidal elements/compounds can adsorb onto particles and be transported downward more rapidly than through settling, diffusional or turbulent mixing, or subduction. Optical measurements have also shown that although particle concentrations in the open ocean decrease to very low values in the water column deeper than about 100-200 m (5-12 µg l^{-1}; Brewer et al., 1976; Gardner et al., 1985), particle concentration can increase near the seafloor, sometimes very significantly (100's-1000's µg l^{-1}: Gardner et al., 1985; Hill et al., 2011). Satellite ocean color data can be used to map particle concentrations globally in surface waters (Gardner et al., 2006; Henson et al., 2010; Stramski et al., 2008). High-resolution vertical measurements throughout the water column primarily depend on CTD hydrocasts, which provide lower horizontal and temporal resolution than satellite data. Profiling floats or gliders with attached optical instruments increase temporal and spatial resolution (Johnson et al, 2009), however most of them presently profile to 2000 m or less. Gliders that will profile to 6000 m are being built. All of these instruments can yield important high-resolution data from multiple sensors simultaneously.

The geographic variability of particle concentrations near the seafloor is orders of magnitude greater than in the mid-water column (Biscaye and Eittreim, 1977). Their synthesis of data in the North and South Atlantic show areas of high concentrations in the

Western North Atlantic and in the Argentine Basin. Their initial hypothesis was that the high concentrations were caused by sediment eroded and resuspended by deep boundary currents generated by polar waters sinking and moving equatorward. Also noted was a spatial association between elevated nepheloid layer particulate matter concentrations (PM) and eddy kinetic energy (EKE) (Hollister and McCave, 1984) or bottom trapped topographic Rossby waves (Grant et al., 1985), however, no global map of bottom concentrations existed. Weatherly and Kelley (1985) suggested that cold filaments of Antarctic Bottom Water were passing through a region south of Nova Scotia in the Western North Atlantic where the dynamics of sediment resuspension was investigated for several years during the High Energy Benthic Boundary Layer Experiment (HEBBLE). The state of general understanding about nepheloid layers 30 years ago was reviewed by McCave (1986), and many of the concepts have not changed. However, most of the data in this paper were collected since that review, giving us a much clearer picture of global geographic distribution, intensity, and variability. New physical measurements and models have also improved our understanding of dynamics in the ocean. In this paper we present the first global maps of bottom particle concentrations, thickness of the nepheloid layer, and integrated particle mass within bottom nepheloid layers compiled from transmissometer data we have collected during the last four decades. We compare these data with global maps of EKE, benthic energy dissipation, mean near-bottom kinetic energy, and refer to newly published time-series measurements in benthic nepheloid layers to better understand the causes, likely location, and variability of strong and weak nepheloid layers.

2. Methods and data

Transmissometers were integrated with CTDs and lowered to the seafloor on 64 cruises occupying 6,392 stations. Transmissometers used in WOCE, JGOFS, SAVE and other open ocean projects up until about year 2000 were 25 cm pathlength, SeaTech instruments with a 660 nm LED light source. One cruise during the HEBBLE program (R/V Knorr cruise 74, 1974) used a 1-m folded pathlength SeaTech instrument, as did one cruise in the Western North Atlantic (R/V Oceanus cruise 134, 1983).

The methods for using the 25-cm path length SeaTech transmissometers are given in papers published for those projects (Gardner et al., 1985, 1993) and in more detail on the Ocean Data View (ODV) web site: https://odv.awi.de/fileadmin/user_upload/odv/data/Transmissometer/info). Explained briefly, a transmissometer measures in volts (0-5 volts (V)) the transmission (T) of light across a path of known length (r). Voltage is then converted to beam attenuation of light (*c*) by the equation:

$$V/5 = T = e^{-cr},$$

which can be rewritten as

$$c = -(1/r) * \ln(T)$$

Data from transmissometers with different path lengths can thus be compared using the same equation.

Light from a red LED is scattered and/or absorbed by water (c_w), particles in the water column (c_p), and colored dissolved organic matter (c_{CDOM}), the sum of which is defined as beam attenuation (c). Thus, $c = c_w + c_{CDOM} + c_p$. In the red spectrum used for our measurements, scattering and absorption by CDOM is considered negligible in most open ocean waters, so attenuation by particles (c_p) equals the total attenuation measured (c) minus the attenuation by water (c_w). SeaTech transmissometers were factory calibrated in particle-free water and the electronics were adjusted so that c_w= 0.364. An initial dry air reading was made at the factory and any drift of the instrument could be detected and corrected by comparison with the air reading in the field during an expedition.

Processing of the data included data averaging (1 or 2 db binning), examination and removal of transient spikes, determination of water column minimum value, adjustments for light source drift based on air readings, and final calibration by regressions of particulate mass (PM) or particulate organic carbon (POC) concentrations versus c_p, when PM or POC data were collected.

We transitioned to WetLabs C-STAR transmissometers in ~ 2000, as SeaTech ceased production and the CLIVAR Repeat Hydrography program started. The WetLabs C-STARs used a 660 nm LED, and the instruments were converted to improved 650 nm LEDs around 2013. Each instrument was factory calibrated in particle-free water and internal firmware was used to subtract attenuation due to water (c_w) from the output data stream. Later WetLabs added an algorithm to correct for instrument internal temperature hysteresis as the external temperature varied quickly in the upper water column. We had developed our own temperature correction with the SeaTech transmissometers (Gardner et al., 1993). The voltage was corrected for drift in the instrument by using factory and field air and blocked beam readings:

$Tr = ((V_{Sig} - V_{Block}) / (V_{Fac} - V_{Block}))*(V_{FacAir} / V_{FieldAir})$,

where - V_{Sig} –is the measured output voltage,

V_{Block} is the output voltage with the beam blocked during calibration,

V_{Fac} – is the factory clean-water value,

V_{FacAir} – is the factory measured voltage output in air,

$V_{FieldAir}$ – is the field measured voltage output in air.

WetLabs C-STAR instruments were used on the CLIVAR Repeat Hydrography/GO-SHIP cruises, but we rarely had the opportunity to collect and filter calibration samples on these cruises, which for us were “ships of opportunity” for data collection. Shipboard technicians were instructed to clean the transmissometer windows prior to each cast and to do a pre-cast air calibration through the CTD every 20 casts and at the beginning and end of the cruise. When FieldBlock and FieldAir are taken several times during the cruise, the calibration values can be linearly interpolated for every day in the cruise between the dates when calibrations occurred and applied to the data. So, if the sensor shift is not linear over the duration of the expedition, it can be accounted for by interpolation.

Without in situ samples we could not establish a known concentration for the minimum values in the water column nor was there particle-free water available on the ship for calibration. Thus we resorted to using the common method proposed by SeaTech of using the cruise minimum voltage or a cruise-average minimum on each cast. We later set this value to zero. This means we can't compare particle minima between oceans, however, the uncertainty in measurements at the low minimum values from many different instruments with many different operators over 4 decades convinced us this was the best solution. Filtration sampling by Brewer et al. (1976) and our own measurements in many oceans shows minimum concentrations of about 5-12 $\mu g\ l^{-1}$. The purpose of this paper is to quantify properties of nepheloid layers such as the thickness and "excess mass" of particles, which requires subtracting the "clear water" concentrations. One could add ~ 12 $\mu g\ l^{-1}$ to obtain total particle concentrations. This would not change the global distribution maps and correlation with ocean dynamics. Furthermore, numerous time-series measurements in the Western North Atlantic show that particle concentrations in active nepheloid layers can change rapidly by over an order of magnitude in a day (Gardner et al., 2017). Even in surface waters, the horizontal variability can be large, so the particle minima of 5-12 $\mu g\ l^{-1}$ are small compared to the typical concentrations in surface waters or active benthic nepheloid layers.

Beam attenuation due to particles (c_p) is linearly correlated with particle concentration, however, c_p is not an intuitive unit and the conversion factor to PM is not a single universal constant, nor is it uniform throughout the water column. This is because beam c_p is a function of particle composition and particle size (Baker and Lavelle, 1984), which change seasonally in surface waters and from surface waters to bottom waters (Gardner, 1989; Gardner et al., 1993; 2001)

Because we are analyzing benthic nepheloid layers, whose primary source of particles is resuspended sediment, there is greater uniformity in the conversion factor from c_p to PM. In order to use a more familiar measurement, we have converted beam c_p to µg l^{-1} using the measurements of nepheloid layer PM from the HEBBLE program (Gardner et al., 1985) because of the large number of samples over the widest range of concentrations in any deep-sea study:

$$PM = 1208 * c_p$$

Data were gridded (1° x 1°), contoured, and displayed using Golden Software's Surfer package. While mapping we tested many search distances from 2° - 15° of longitude/latitude and found that using a search radius of 6.5° was optimal in terms of data presentation without excessive small-scale details and interpolation artifacts. Because of this, highest PM values are not obvious. We have included a figure in Appendix A that maps stations based on near-bottom concentration ranges in µg l^{-1} (>1000, 1000-500, 500-100, 100-50, 50-10, <10).) The greater the near-bottom concentration, the more variable concentrations are likely to be (Gardner et al., 2017). When a location is occupied more than once, the data are averaged in the gridding.

The "maximum bottom concentration" at each station was determined by taking an average of the bottom 10 m of data collected. The distance above bottom for each cast is not always reported, however, most cruise logs show it is generally 5-10 meters above bottom (mab). In the HEBBLE program the distance was narrowed to 2-7 mab using a weighted touch wire that triggered a red light on the CTD control panel at 2 mab.

The minimum concentration in the profile is calculated for each station, however, the minimum can occur at multiple depths. Mapping the depths of the deepest minimum led to vary erratic contours. Erratic contours also occurred by using an increase of 0.005 c_p below the minimum to define the beginning of the nepheloid layer. When we used an increase of 0.01 c_p there was much less noise in the maps. The depth of the minimum plus 0.01 c_p units was used to define the top of the nepheloid layer (which is an increase of about 12 μg l^{-1}), and the excess PM in the nepheloid layer was obtained by integrating from that depth to the deepest measurement. No addition was made for the mab of a cast as there was too much uncertainty in that distance, which was usually only ~5-10m.

CTD/Transmissometer data up until 2012 are available at National Centers for Environmental Information (NCEI) (http://www.nodc.noaa.gov/OC5/WOD13/) and at the Ocean Data View web site (http://odv.awi.de/en/data/ocean/). Data from 2003 to present are being uploaded to the CCHDO database (https://cchdo.ucsd.edu). All of the JGOFS transmissometer data we collected can be found at http://usjgofs.whoi.edu/jg/dir/jgofs/.

Our CTD/transmissometer stations seldom include measurements on the shelf, however, there are many studies that show resuspension of bottom sediments in shallow environments that will not be covered here. Sediment has also been shown to be resuspended by breaking internal waves on tidal cycles on the upper slope and in submarine canyons, creating intermediate nepheloid layers (Gardner, 1989 and refs therein), however, there is no direct evidence that this sediment from the upper slope contributes significantly to benthic nepheloid layers in the deep sea. There are also many measurements in the Mediterranean Sea (Karageorgis et al., 2008: Puig et al., 2013;) and Gulf of Mexico (Son et al., 2009). We have not included those in our data set, though we recognize the importance of those marginal seas.

3. Results and Discussion

3.1. Maximum concentration, thickness and excess PM in nepheloid layers.

The global distribution of maximum near-bottom PM concentrations reveals significant spatial variability (Fig. 1). Two large open-ocean areas where the maximum bottom PM concentrations frequently exceeded 100 µg l^{-1} (total of 387 stations globally, Appendix A1-A3) are the Western North Atlantic Basin and Argentine Basin. The stations with high concentrations north of Alaska and north of the Amazon outflow are shallow water stations (<400 m). There are profiles in other places that had concentrations >100 µg l^{-1}, but since we use 1° gridding, higher concentration data points can be smoothed out. Concentrations sometimes exceeded 1,000 µg l^{-1} at several stations south of Nova Scotia in the North Atlantic below the Gulf Stream and its extensions. Maximum value from filtered samples in that region was 12,701 µg l^{-1} at 2 mab and values exceeded 2,000 µg l^{-1} as high as 131 mab at that site (Gardner and Sullivan, 1981). The c_p profile at that station showed more than one maximum in the bottom waters that was generated either by advection from higher topography nearby, or, in retrospect, it is possible that we sampled the tail end of a turbidity current. The beam attenuation (c) signal was saturated (c=8.9 for 1-m pathlength transmissometer) in the bottom 20 m.

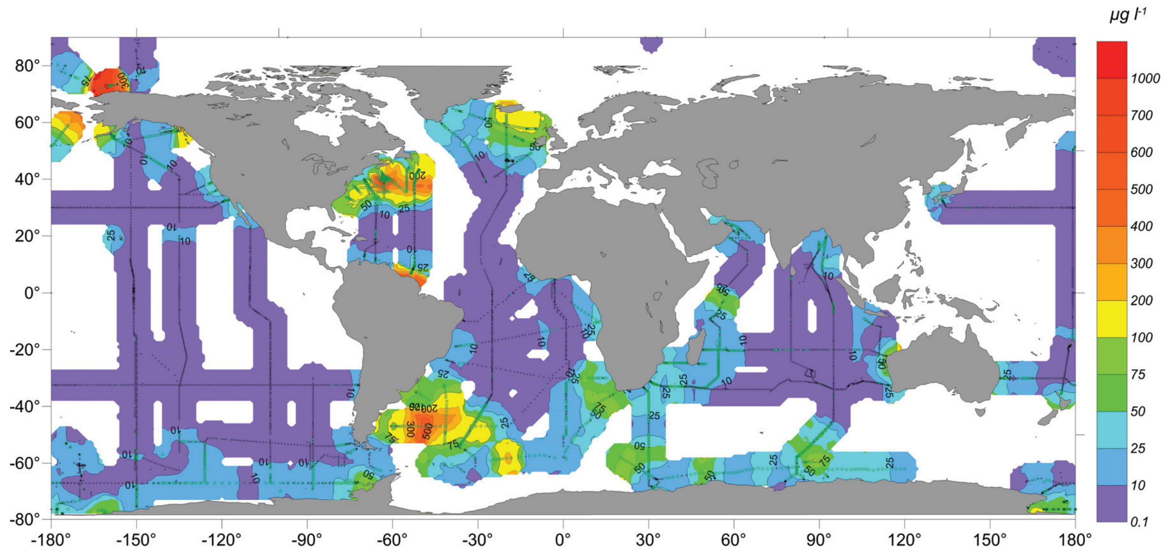

Figure 1. Particulate matter concentration (µg l^{-1}) averaged in the bottom 10 m of each profile. Scale is not linear to provide finer detail at low concentrations. Data were gridded at 1° x 1° areas and a search radius of 6.5° was used for interpolation. In Figs. 1-4, black symbols indicate stations where no nepheloid layer was observed (i.e. no concentration increase by >12 µg l^{-1}). Green symbols indicate stations where an increase of 12 µg l^{-1} greater than the profile minimum was observed.

Smaller areas with high PM concentrations include south of Iceland and southwest and southeast of Alaska (shallow water). Medium PM values (50-100 µg l^{-1}: 413 stations globally, Appendix A4) also occur sporadically in the Southern Ocean, southwest of Africa and northeast of Madagascar. It is notable that much of the ocean has very low PM concentrations (<10 µg l^{-1} Appendix A6), indicating little or no sediment resuspension. The transects covered in this paper were seldom close to mid-ocean ridges, where hundreds of hydrothermal vents are manifest as increased temperature, turbidity, iron or other elements (Baker, 2017; Fitzsimmons et al., 2017). These areas aren't obvious in our maps.

The thickness of the nepheloid layer is defined here as the distance between the c_{p_min}+0.01 depth and the profile bottom depth (Fig. 2). This is to ensure that there is a real increase in PM, since that is at the low end of the instrument's resolution. The excess PM mass is calculated by integrating the PM mass within the entire nepheloid layer (Fig. 3), which gives a more robust evaluation of erosion and resuspension of bottom sediments than just the average concentration in the bottom 10 m. The areas in the Western North and South Atlantic where bottom concentrations exceeded 500 $\mu g\ l^{-1}$ (Fig. 1, Appendix A1, A2) and the nepheloid layer thickness exceeds 500 m (Fig. 2) generally coincide with areas where integrated excess PM mass exceeds ~4000 $\mu g\ cm^{-2}$.

In the maps of both integrated excess mass and nepheloid layer thickness, the area beneath the Agulhas retroflection southwest of Africa shows up more prominently than in bottom PM concentrations. Similarly, nepheloid layer thickness in areas south and east of Madagascar are greater than most regions of the ocean indicating that resuspended sediment was advected there from the lower continental slope and upper rise.

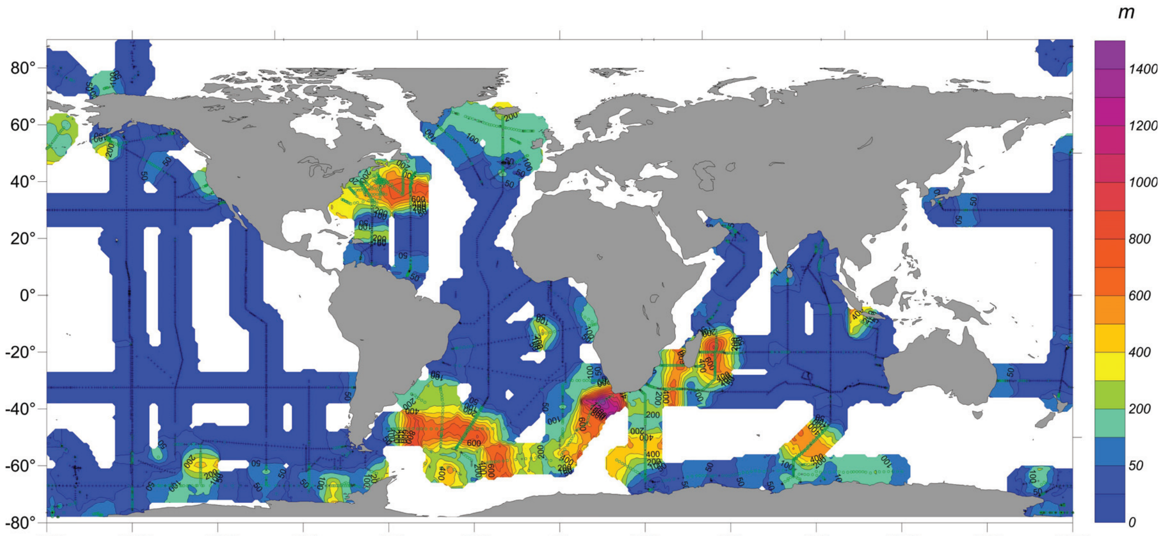

Figure 2. Thickness of the nepheloid layer (m). Note scale change at 200 m.

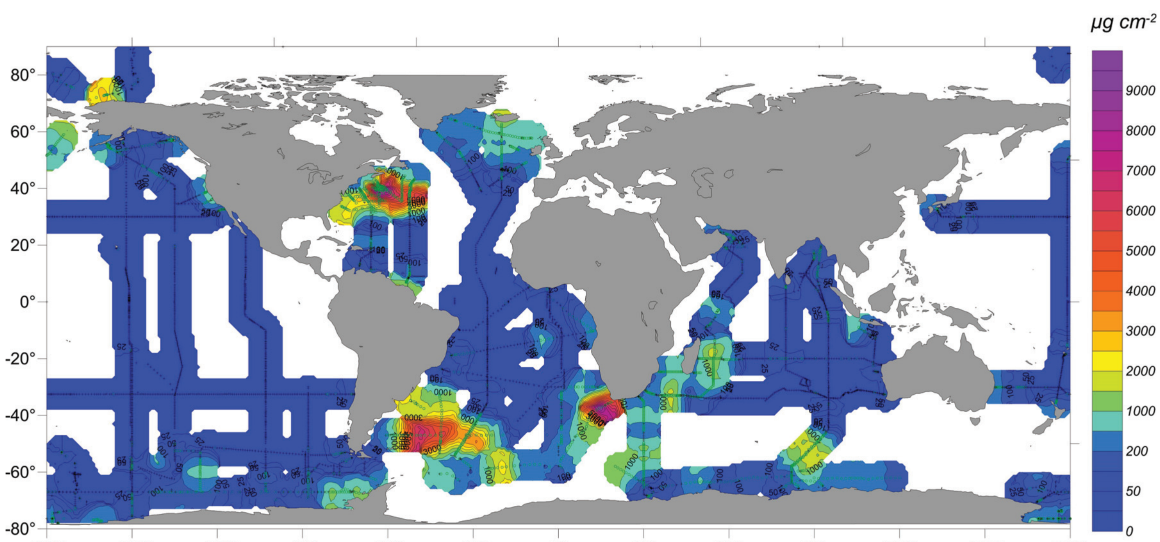

Figure 3. Excess particulate matter in the nepheloid layer (μg cm^{-2}). Note scale change at 1000 μg cm^{-2}. See section 2 for calculation.

A paper by Homoky et al. (2016, Fig. 12g) showed a map of excess PM in the nepheloid layer, citing Biscaye and Eittreim (1977). However, the Biscaye and Eittreim paper contained data only for the North and South Atlantic, not global data. The global data in Homoky et al. (2016) were not “optical transmission measurements.” They were forward scattering white light data compiled from Lamont nephelometer archives long ago by Biscaye and Gardner, preserved in an LDEO data base called GeoMapApp, and presented by us at the 2014 Ocean Sciences meeting in Hawaii. The Lamont nephelometer data are compared with the transmissometer data presented here in a paper soon to be submitted.

Testing for correlations, we examined linear regressions of the integrated excess PM versus maximum bottom PM concentration and nepheloid layer thickness. We found a general positive correlation (which was not always linear, had highly variable regression slopes geographically, and had considerable scatter in the data) in regressions for either individual cruises or areas, but when all global data were combined, there was too much scatter to generalize the relationship globally (data not shown). This suggests that different areas have different forcing functions that give rise to the diverse structure and intensity of benthic nepheloid layers.

3.2. Areas of strongest nepheloid layers and synopticity

The two areas of maximum PM in Figures 1 and 3 were highlighted in the Biscaye and Eittreim (1977) map of the North and South Atlantic. In their map the area southwest of Africa showed slightly elevated mass in the nepheloid layer, however concentrations were much higher when our transmissometer data were collected two decades later. It is important to note that the data of Biscaye and Eittreim (1977) were measurements of forward-scattered white light regressed against filtered particle concentrations in bottom waters in the Western North Atlantic and converted to mass concentrations. Our beam attenuation data are optical measurements that have been regressed against particle concentrations in bottom waters south of Nova Scotia during the HEBBLE program and the regression obtained was used to convert c_p values to particle mass concentrations. The only place or time where a transmissometer and the Lamont Nephelometer have been deployed simultaneously was during R/V Knorr HEBBLE cruise KN74 and during a 2.5 month deployment of a bottom tripod with both instruments collecting data simultaneously at the same time about 1 m off the bottom (Gardner et al., 1985; 2017). For all assessments in this paper we are comparing PM concentrations to PM concentrations, rather than one optical measurement to another.

Our transmissometer data were collected over a 38-year period in various seasons, and are contoured as if all were collected simultaneously. Two pieces of strong evidence that justify our combining the data over multiple years are 1) we found areas of high PM concentration in the same two areas of highest concentration in Biscaye and Eittreim (1977) in the ‘70’s – ‘80’s, and 2) all of the beam c_p sections that we have made from transects repeated 10-20 years apart in different oceans have shown that high and low benthic PM concentrations occur in the same areas during each transect (Gardner et al., 2016). It has long been recognized that benthic nepheloid layers result primarily from resuspension of bottom sediment somewhere, or along mid-ocean ridges from hydrothermal vents (Baker, 2017). See Puig et al., (2013) for a third mechanism for forming benthic nepheloid layers - cascading of dense shelf water. The high and low concentrations during different decades consistently occur in the same regions, suggesting that there are regional hydrodynamic forces and/or topography that generate currents strong enough in specific locations to erode and resuspend sediment, and in other locations currents are rarely strong enough to erode or resuspend bottom sediments.

Are there seasonal variations in the PM concentration in nepheloid layers that might create a bias in the data? There is evidence from time-series photographs (Lampitt, 1985) and sediment trap data (Deuser, 1980) that many areas of the ocean experience seasonal variations in the downward flux of organic detritus from surface waters, however, we know of no evidence of seasonality in near-bottom PM concentrations other than seasonal cascading of water in the Mediterranean (Puig et al., 2013). Nor is there evidence for seasonal variations in bottom currents sufficient to resuspend sediments and create areas of intense nepheloid layers. Certainly there is seasonality in the formation of bottom waters in polar regions, however, mean flow of the Deep Western Boundary Current (DWBC) is only about 10 cm s^{-1} and seasonal increases in bottom currents of the DWBC are only about 10-20% (Dickson et al., 2007; Jochumsen et al., 2012). Episodic benthic storms have been documented in the Western North Atlantic (Gardner and Sullivan, 1981; Gardner et al., 2017; Hollister and McCave, 1984; Isley et al. 1990), however, there is no evidence of a seasonal bias in their occurrence.

3.3. Causes of intense nepheloid layers

Hollister and McCave (1984) pointed out a general global correlation between deep boundary currents, strong nepheloid layers and high surface eddy kinetic energy generated by features such as the Gulf Stream and its warm and cold-core rings, suggesting that sediment resuspended could be diffused upward or advected laterally.

Bottom boundary layer thickness is usually less than 100 m, depending on bottom topography, slope, and current speeds (Armi and Millard, 1976), yet nepheloid layers can be as thick as 1000-1400 m (Fig. 2). It is more likely that sediment is advected laterally as demonstrated by Armi (1978) to create thick nepheloid layers because eddy diffusivity required to explain diffusional mixing for clay particles up to 1000–1500 mab is two orders of magnitude greater than the typical vertical diffusivities of 1 cm^2 s^{-1} calculated for most of the deep ocean (Bell, 1974; Eittreim and Ewing, 1972). Later studies by Watts et al. (1995) and Andres et al. (2016) have shown that beneath the meanders of the Gulf Stream, cyclones and anticyclones are generated that create currents strong enough to resuspend sediment in waters much deeper than the DWBC, which extends only to ~4000 m depth in the Western North Atlantic with the water deeper than 4000 m consisting mainly of Antarctic Bottom Water (AABW) based on high silicate concentrations (Richardson et al., 1981).

We presented extensive new data and analysis on nepheloid layer distribution and dynamics in the Western North Atlantic basin based on Lamont nephelometer data (Gardner et al., 2017). We mapped the excess PM in nepheloid layers from vertical profiles and collected near-bottom time-series measurements (2-11 months each) of particle concentrations that revealed numerous benthic storms beneath the Gulf Stream, many of which were associated with nearby meanders and rings. We also compared the surface EKE with PM concentrations and temporal variability in benthic PM concentration and found a tight correlation. The high concentrations Biscaye and Eittreim (1977) mapped from nephelometer data in the '70's – '80's match well the high values seen based on these transmissometer measurements from 1979-2016 (Figures 1-3). We concluded that the DWBC speeds were too weak by themselves to generate intense nepheloid layers. Benthic storms with current speeds >~20 cm s^{-1}, caused by cyclogenesis or bottom-trapped topographic Rossby waves were required to erode the seafloor and maintain moderate to strong benthic nepheloid layers. We also found that benthic nepheloid layers are weak to non-existent in areas of low eddy kinetic energy.

Another hypothesis for resuspension of bottom sediments in the Western North Atlantic was proposed by Weatherly and Kelley (1985). They detected cold filaments containing AABW beneath the Gulf Stream moving up and down the deep slope and the filaments were sometimes associated with increases in PM. They could detect the shoreward boundary of the filaments, but not the offshore boundary and suggested that this movement of cold water is part of an abyssal western boundary current in the North American Basin or of a basin-scale cyclonic or anti-cyclonic circulation (Hogg, 1983) in the Western North Atlantic. However, Weatherly and Kelley (1985) also presented sections from previous studies in the same area that looked similar to the cold filaments, but those sections included an offshore boundary so isotherms formed a dome that could be interpreted as a cold filament meandering along the deep slope. We suggest an alternative interpretation that rather than it being a continuous filament flowing as part of the DWBC, the sections could bisect cyclonic features generated by the Gulf Stream meanders. Cyclonic rotation could cause upwelling in the center of the cyclone, thus carrying cold water and resuspended sediment upward, though not hundreds of meters. Lateral mixing away from boundaries is still required to develop nepheloid layers hundreds of meters thick. This could occur along continental margins or as water moves past seamounts and smaller hills in the ocean that Turnewitsch et al., (2013) point out are more abundant than is generally recognized.

A map of global surface EKE (data generated by the joint U.S.-French TOPEX/POSEIDON and the JASON Ocean Surface Topography Science Teams (OST/ST)) was visualized by Dixon et al., (2011) and reveals marked similarities between surface EKE and benthic nepheloid layer intensity (Fig. 4). In addition to the Western North Atlantic, good correlation between EKE and nepheloid layer intensity is found in the Argentine Basin as previously noted by Hollister and McCave (1984). Time series transmissometer and current measurements near the seafloor also provided evidence of benthic storms in that basin that are correlated with high surface EKE caused by confluences, meanders, and eddies spun off from the Brazil (southward flowing) and Malvinas (northward flowing) boundary currents (Richardson et al., 1993). Flow between Madagascar and Africa occurs in eddies rather than a steady current (Penven et al., 2006). Then the Agulhas Current spawns rings at the Agulhas retroflection south of Africa. This eddying motion correlates well with relatively strong nepheloid layers from Madagascar around the Horn of Africa to southwest of Africa where concentrations are most intense where the current reverses course and moves to the southeast (Figs. 2, 3).

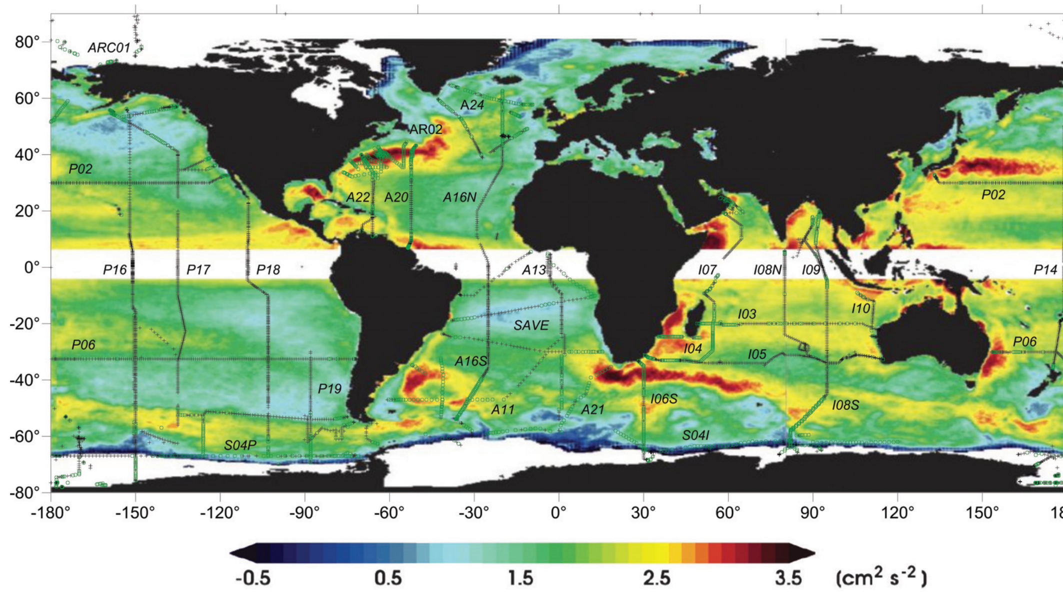

Figure 4. Map of log of surface EKE based on satellite observations during 2002-06 (modified from Dixon et al., 2011) with transmissometer station locations superimposed and WOCE lines annotated.

3.4. Are there nepheloid layers beneath the Kuroshio?

The greatest anomaly when comparing surface EKE and benthic nepheloid layers based on existing data is the area beneath the Kuroshio Current off of Japan. Like the Gulf Stream, the Kuroshio is a strong surface western-boundary current that meanders and sheds eddies in a manner similar to the Gulf Stream. One topographic difference is that the Japan Trench (~10,000 m) underlies the western flank of the Kuroshio, whereas the continental rise underlies the Gulf Stream and the Brazil/Malvinas currents in the Argentine Basin. Meandering of the Kuroshio begins northeast of the trench and moves to the northeast where water depth is 5000-6000 m. Extensive current measurements between 33°-37° N beneath the main flow of the Kuroshio revealed intensified bottom flow in the entire region that was weakly bottom trapped (Bishop et al., 2012). Near isolated seamounts, both currents and bottom trapping were amplified. Current speeds were measured at 2000, 3500 and 5000 m at five sites for nearly two years and the coherence of speeds among those three depths was very high. Speeds were filtered to remove tidal influence and still the speed frequently exceeded 20 cm s^{-1}, which is the speed at which erosion/resuspension was found to occur beneath the Gulf Stream (Gardner et al., 2017). In this region Greene et al. (2009) found that cyclogenesis can result from strong flows advecting water columns off of isolated seamounts following a quiescent interval, so that could enhance current speeds, which reached a maximum of about 25 cm^{-1} at all depths. Thus, the conditions were such that strong nepheloid layers would be expected.

Another difference between the water column beneath the Kuroshio and that of the Gulf Stream is that no DWBC flows counter to the Kuroshio’s surface current because no bottom water is formed in the north Pacific. However, Gardner et al., (2017) established that the DWBC flow beneath the Gulf Stream is too slow and too shallow (maximum 4000 m) to create benthic storms found at 4500-5200 m. Still, one would expect the same type of cyclones and anticyclones beneath the Kuroshio that exist at 5200 m beneath meanders and rings of the Gulf Stream.

A third critical difference with the Kuroshio is a lack of PM data. We have no transmissometer profiles beneath the area of high EKE (Fig. 4), and no time-series measurements of PM near the seafloor. We have two occupations of the east-west section along 30°N (Fig.4, line PO2), but this is south of the Kuroshio where we would expect nepheloid layers to develop (~35°N). However, bottom photos at two stations beneath the Kuroshio showed a smoothed bottom or mounds with tails (Fig. 1 of Hollister and Nowell, 1991), which is evidence of sediment transport and resuspension at some time in the past.

3.5. Other correlations between nepheloid layers and seafloor dynamics

In addition to looking at surface EKE, assimilation of thousands of current measurements with eddying general circulation models and tides has yielded detailed global maps of mean kinetic energy 50 mab (Fig. 2 of Arbic et al., 2010) as well as equally detailed global maps of energy dissipation in the bottom boundary layer (Figs. 5 and 9 of Arbic et al., 2009; Fig. 3 of Wright et al., 2013). There is significant agreement between their maps of energy dissipation and the maps of surface EKE (Fig. 4) in the vicinity of the Gulf Stream, the Agulhas current, in the Argentine Basin, and in spots beneath the Antarctic Circumpolar Current. Given that the areas of higher EKE in the circumpolar current are likely due to eddies (Chelton et al., 2007), their geographic location may be less constrained than in the areas of high EKE unless there are topographic features like the Drake Passage or Kerguelen Islands where eddies might be generated regularly.

Observations also show high energy dissipation rates due to bottom boundary drag beneath the Kuroshio between 32°-38°N. Conversely, maps of modeled mean kinetic energy at 50 mab show similarly maximum values in all of the regions of high EKE except beneath the Kuroshio where mean kinetic energy is about half of that beneath the Gulf Stream and Argentine Basin currents (Arbic et al., 2010; Fig. 2), yet currents are strong enough to erode sediment. More data are needed to know if there are strong nepheloid layers beneath the meandering portion of the Kuroshio, and if not, why?

3.6. Practical applications

In addition to obtaining a better understanding of the impact of surface dynamics on deep currents and eddies and sediment erosion and transport, this synthesis of nepheloid layers has other important applications. There is continued and growing interest and engineering effort focusing on mining metal-rich nodules and massive metallic sulfides on the seafloor (Halfar and Fujita, 2002; Hoagland et al., 2010; Van Dover, 2014). Deep-sea mining introduces particulate matter into the water column, either near the surface, seafloor, or in the water column. We want to be able to differentiate these 'industrial' sources from natural processes of resuspension for a variety of reasons. Our maps and analysis provide baseline data to understand where, when, why and how much PM we can expect in different geographic locations and in each part of the water column due to settling of particles from surface waters, by natural erosion and resuspension of bottom sediments, and input from hydrothermal activity. With the information in our synthesis, the location and impact of mining on the benthic environment can be better identified.

Furthermore, studies in the Geochemical Tracers program (GEOTRACES) have found that PM scavenges adsorption-prone radionuclides such as ^{230}Th and ^{231}Pa that are used as quantitative tracers of adsorption to sinking particles in the ocean (Hayes et al., 2015; Van Hulten et al., 2017). These radionuclides have been used as modern- and paleo-proxies for estimating vertical fluxes to the seafloor and lateral fluxes of insoluble elements to the continental margins as well as understanding the southward flux of North Atlantic deep water and other aspects of ocean circulation. Our improved understanding of which driving forces are important (EKE, topographic waves, cyclones and anticyclones spun up beneath meanders and rings of strong boundary currents) and where PM in the benthic nepheloid layer is sourced, transported, and deposited will help to determine oceanic locations where such scavenging is most likely to occur and to assess its impact on present and past global biogeochemistry.

4. Conclusions

Benthic nepheloid layers are most intense beneath areas of high surface eddy kinetic energy, strongly suggesting a linkage with upper ocean dynamics. The geographic locations of intense nepheloid layers also coincide with areas of high-energy dissipation in the bottom boundary layer and with mean kinetic energy at 50 mab. One anomaly of this correlation may be the Kuroshio Current where we have current data, but no PM data. The energy dissipation is high beneath the Kuroshio, however, mean kinetic energy at 50 mab is not as high there as in other areas of high benthic PM. PM data are needed to resolve the anomaly.

Bottom boundary currents are too weak to generate intense nepheloid layers, so bottom current intensification (benthic storms) created by cyclones/anticyclones beneath meanders/rings below major surface currents or from bottom-trapped topographic waves is required to episodically create and maintain intense nepheloid layers. Benthic nepheloid layers in large portions of the Pacific, Atlantic and Indian oceans are weak to non-existent and are areas of low eddy kinetic energy. There are still many geographic areas to explore.

PM scavenges adsorption-prone radionuclides that are used as paleo-productivity proxies and for investigation and modeling of modern and paleo-ocean circulation. Our global maps of PM in the benthic nepheloid layer help to determine where such scavenging is most likely to occur and to assess its potential impact on global biogeochemistry of sediments and bottom water. These maps will also serve as a baseline as deep-sea mining expands to exploit more mineral resources.

References

Andres, M., Toole, J.M., Torres, D.J., Smethie Jr., W.M., Joyce, T.M., Curry, R.G., 2016. Stirring by deep cyclones and the evolution of Denmark Strait overflow water observed at line W. Deep-Sea Research Part I, Oceanographic Research Papers 109, 10-26.

Arbic, B.K., Shriver, J.F., Hogan, P.J., Hurlburt, H.E., McClean, J.L., Metzger, E.J., Scott, R.B., Sen, A., Smedstad, O.M., Wallcraft, A.J., 2009. Estimates of bottom flows and bottom boundary layer dissipation of the oceanic general circulation from global high-resolution models. Journal of Geophysical Research 114, C02024, doi:10.1029/2008JC005072.

Arbic, B.K., Wallcraft, A.J., Metzger, E.J., 2010. Concurrent simulation of the eddying general circulation and tides in a global ocean model. Ocean Modeling 32, 175 - 187.

Armi, L., 1978. Mixing in the deep ocean - the importance of boundaries. Oceanus 21, 14-19.

Armi, L., Millard Jr, R.C., 1976. The bottom boundary layer of the deep ocean. Journal of Geophysical Research 81, 4983–4990, doi:10.1029/JC081i027p04983.

Baker, E.T., Lavelle, J.W., 1984. The effect of particle size on the light attenuation coefficient of natural suspensions. Journal of Geophysical Research 89: 8197-8203.

Baker, E.T., 2017. Exploring the ocean for hydrothermal venting: New techniques, new discoveries, new insights. Ore Geology Reviews 86, 55–69, doi: 10.1016/j.oregeorev.2017.02.006

Bell, T.H., 1974. Vertical mixing in the deep ocean. Nature 251, 43-44.

Biscaye, P.E., Eittreim, S.L., 1977. Suspended particulate loads and transports in the nepheloid layer of the abyssal Atlantic Ocean. Marine Geology 23, 155-172.

Bishop, S. P., Watts, D. R., Park, J-H, Hogg, N.G., 2012. Evidence of Bottom-Trapped Currents in the Kuroshio Extension Region, Journal of Physical Oceanography 42, 321-328.

Brewer, P.G., Spencer, D.W., Biscaye, P.E., Hanley, A., Sachs, P.S., Smith, C.L., Kadar, S., Fredericks, J., 1976. The distribution of particulate matter in the Atlantic Ocean. Earth and Planetary Science Letters 32, 393-402.

Chelton, D. B., Schlax, M.G., Samelson, R.M. de Szoeke, R.A., 2007. Global observations of large oceanic eddies, Geophysical Research Letters 34, L15606, doi:10.1029/2007GL030812.

Deuser, W. G., Ross, E. H., 1980. Seasonal change in the flux of organic carbon to the deep Sargasso Sea, Nature 283, 364-365.

Dickson, R.R., Rudels, B., Dye, S., Karcher, M., Meincke, J., Yashayaev, I., 2007. Current estimates of freshwater flux through Arctic and subarctic seas. Progress in Oceanography 73, 210-230.

Dixon, K.W. Delworth, T.L., Rosati, A.J., Anderson, W., Adcroft, A., Balaji, V., Benson, R., Griffies, S.M., Lee, H-C., Pacanowski, R.C., Vecchi, G.A., Wittenberg, A.T., Zeng, F., Zhang, R., 2011. Ocean circulation features of the GFDL CM2.6 & CM2.5 high-resolution global coupled climate models. WCRP Open Science Conference, October 2011, Denver, Colorado.

Eittreim, S. Ewing, M., 1972. Suspended particulate matter in the deep waters of the North American Basin, in Gordon, A. L. (Ed.), Studies in Physical Oceanography. Gordon and Breach, London, pp. 123-167.

Fitzsimmons, J.N., John, S.G., Marsay, C.M., Hoffman, C.L., Nicholas, S.L., Toner, B.M., German, C.R., Sherrell, R.M., 2017. Iron persistence in a distal hydrothermal plume supported by dissolved-particulate exchange. Nature Geoscience. 10, 195-201, doi:10.1038/ngeo2900.

Gardner, W. D., 1989. Periodic resuspension in Baltimore Canyon by focusing of internal waves. Journal of Geophysical Research 94:18185-18194.

Gardner, W.D., Biscaye, P.E., Zaneveld, J.R.V., Richardson, M.J., 1985. Calibration and comparison of the LDGO nephelometer and the OSU transmissometer on the Nova Scotian Rise. Marine Geology 66, 323-344, 1985a.

Gardner, W. D., Blakey, J. C., Walsh, I.D., Richardson, M.J., Pegau, S., Zaneveld, J.R.V., Roesler, C., Gregg, M.C., MacKinnon, J. A., Sosik, H.M., Williams, A. J., III, 2001. Optics, particles, stratification and storms on the New England continental shelf. Journal of Geophysical Research 106: 9473-9497.

Gardner, W.D., Richardson, M.J., Mishonov, A. V., 2016. Global Distribution and Intensity of Deep-Water Benthic Nepheloid Layers, Ocean Sciences Meeting in February 2016, New Orleans, LA.

Gardner, W.D., Sullivan, L.G., 1981. Benthic storms: Temporal variability in a deep ocean nepheloid layer. Science 213, 329-331.

Gardner, W.D., Tucholke, B.E., Richardson, M.J., Biscaye. P.E., 2017. Benthic storms, nepheloid layers, and linkage with upper ocean dynamics in the Western North Atlantic. Marine Geology 385, 304-327, http://dx.doi.org/10.1016/j.margeo.2016.12.012

Gardner, W.D. Mishonov, A.V., Richardson, M.J., 2006, Global POC concentrations from in-situ and satellite data. Deep-Sea Research II 53, 718-740. DOI: doi:10.1016/j.dsr2.2006.01.029

Gardner, W. D., Walsh, I.D., Richardson, M J., 1993. Biophysical forcing of particle production and distribution during a spring bloom in the North Atlantic. Deep-Sea Research 40, 171-195.

Grant, W.D., Williams III, A.J., Gross, T.F.A., 1985. Description of the bottom boundary layer at the HEBBLE site: Low frequency forcing, bottom stress and temperature structure. Marine Geology 66, 219-241.

Greene, A.D., Sutyrin, G.G, Watts, D.R., 2009. Deep cyclogenesis by synoptic eddies interacting with a seamount. Journal of Marine Research 67, 305–322.

Halfar J., Fujita R.M., 2002. Precautionary management of deep-sea mining. Marine Policy 26, 103–106.

Hayes, C.T., Anderson, R.F., Fleisher, M.Q., Huang, K.-F., Robinson, L.F., Lu, Y., Cheng, H., Edwards, R.L. Moran, S.B., 2015. ^{230}Th and ^{231}Pa on GEOTRACES GA03, the U.S. GEOTRACES North Atlantic transect, and implications for modern and paleoceanographic chemical fluxes. Deep Sea Research Part II: Topical Studies in Oceanography 116, 29-41, doi:http://dx.doi.org/10.1016/j.dsr2.2014.07.007.

Henson, S.A., Sarmiento, J.L., Dunne, J.P., Bopp, L., Lima, I., Doney, S. C., John, J., Beaulieu, C., 2010. Detection of anthropogenic climate change in satellite records of ocean chlorophyll and productivity. Biogeosciences 7, 621–640, 2010.

Hill, P.S., Boss, J E., Newgard, P., Law, B.A., Milligan, T.G., 2011. Observations of the sensitivity of beam attenuation to particle size in a coastal bottom boundary layer, Journal of Geophysical Research 116, C02023, doi:10.1029/2010JC006539

Hoagland, P., Beaulieu, S., Tivey, M.A., Eggert, R.G., German, C., Glowka, L., Lin, J., 2010. Deep-sea mining of seafloor massive sulfides. Marine Policy 34, 728–732.

Hogg, N.G., 1983. A note on the deep circulation of the Western North Atlantic: its nature and causes. Deep-Sea Research Part A. Oceanographic Research Papers. 30, 945-961.

Hollister, C.D., McCave, I.N., 1984. Sedimentation under deep-sea storms. Nature 309. 220-222.

Hollister, C.D., Nowell, A.R.M., 1991. HEBBLE epilogue. Marine Geology. 99, 445-460.

Homoky W.B., Weber, T., Berelson, W.M., Conway, T.M., Henderson, G.M., van Hulten, M., Jeandel, C., Severmann, S., Tagliabue, A., 2016. Quantifying trace element and isotope fluxes at the ocean-sediment boundary: a review. Philosophical Transactions of the Royal Society of London A 374: 20160246. http://dx.doi.org/10.1098/rsta.2016.0246

Isley, A.E., Pillsbury, R.D., Laine, E.P., 1990. The genesis and character of benthic turbid events, northern Hatteras Abyssal Plain. Deep-Sea Research 37, 1099-1119.

Jerlov, N.C., 1953, Particle distribution in the ocean. Reports of the Swedish Deep-Sea Expedition 3, 73-97.

Johnson, K.S., Berelson, W.M., Boss, E.S., Chase, Z., Claustre, H., Emerson, S.R., Gruber, N., Körtzinger, A., Perry, M.J., Riser, S.C., 2009. Observing biogeochemical cycles at global scales with profiling floats and gliders: prospects for a global array. Oceanography 22, 216-225.

Jochumsen, K., Quadfasel, D., Valdimarsson, H., Jónsson, S., 2012. Variability of the Denmark Strait overflow: Moored time series from 1996–2011. Journal of Geophysical Research 117, C12003, doi:10.1029/2012JC008244, 2012.

Karageorgis, A., Gardner, W.D., Georgopoulos, D., Mishonov, A.V., Krasakopoulou, E., Anagnostou, C., 2008. Particle dynamics in the Eastern Mediterranean Sea: a synthesis based on light transmission. PMC and POC archives (1991-2001), Deep-Sea Research I 55: 177-202. DOI: 10.1016/j.dsr.2007.11.002.

Lampitt, R.S., 1985. Evidence for the seasonal deposition of detritus to the deep-sea floor and its subsequent resuspension. Deep-Sea Research 32, 885–897.

McCave, I.N., 1986. Local and global aspects of the bottom nepheloid layers in the world ocean, Netherlands Journal of Sea Research. 20 167-181.

Penven, P. Lutjeharms, J.R.E., Florenchie, P., 2006. Madagascar: A pacemaker for the Agulhas Current system? Geophysical Research Letters. 33 L17609. doi:10.1029/2006GL026854.

Puig, P., Durrieu de Madron, X., Salat, J., Schroeder, K., Martín, J., Karageorgis, A.P., Palanques, A., Roullier, F., Lopez-Jurado, J.L., Emelianov, M., Moutin, T. Houpert, L., 2013. Thick bottom nepheloid layers in the western Mediterranean generated by deep dense shelf water cascading. Progress in Oceanography 111, 1-23.

Richardson, M.J., Weatherly, G.L., Gardner, W.D., 1993. Benthic storms in the Argentine Basin. Deep-Sea Research 40 975-987.

Richardson, M.J., Wimbush, M., Mayer, L., 1981. Exceptionally strong near-bottom flows on the continental rise of Nova Scotia. Science 213, 887-888.

Son*, Y.B., W.D. Gardner, A.V. Mishonov, and M.J. Richardson, 2009. Multispectral Remote Sensing Algorithms for Particulate Organic Carbon (POC): the Gulf of

Mexico, Remote Sensing of Environment 113:50–61. DOI: 10.1016/j.rse.2008.08.011

Stramski, D., Reynolds, R. A., Babin, M., Kaczmarek, S., Lewis, M. R., Röttgers, R. Sciandra, A, Stramska, M, Twardowski, M.S. Claustre, H., 2008. Relationship between the surface concentration of particulate organic carbon and optical properties in the eastern South Pacific and eastern Atlantic Oceans. Biogeosciences 5, 171−201.

Turnewitsch, R., Falahat, S., Nycander, J., Dale, A., Scott, R.B., Furnival, D., 2013. Deep-sea fluid and sediment dynamics—Influence of hill- to seamount-scale seafloor topography. Earth-Science Reviews 127, 203–241.

Van Dover, C.L., 2014. Impacts of anthropogenic disturbances at deep-sea hydrothermal vent ecosystems: a review. Marine Environmental Research 102, 59–72. http://dx.doi.org/10.1016/j.marenvres.2014.03.008.

Van Hulten, M.M.P., Dutay, J.-C. Roy-Barman, M., 2017. Ocean model of Protactinium, Thorium and Particles (ProThorP). https://doi.org/10.5281/zenodo.1009064.

Watts, D.R., Tracey, K.L., Bane, J.M., Shay, T.J., 1995. Gulf Stream path and thermocline structure near 74°W and 68°W. Journal of Geophysical Research, Oceans 100, 18,291-18,312.

Weatherly, G.L., Kelley, E.A., 1985. Two views of the cold filament. Journal of Physical Oceanography 15, 68-81.

Wright, C.J., Scott, R.B., Furnival, D., Ailliot, P., Vermet, F., 2013. Global observations of ocean-bottom subinertial current dissipation. Journal of Physical Oceanography 43, 402-417. doi: 10.1175/JPO-D-12-082.1

Figure Captions

Figure 1. Particulate matter concentration (µg l^{-1}) averaged in the bottom 10 m of each profile. Scale is not linear to provide finer detail at low concentrations. Data were gridded at 1° x 1° areas and a search radius of 6.5° was used for interpolation. In Figs. 1-4, black symbols indicate stations where no nepheloid layer was observed (i.e. no concentration

increase by >12 $\mu g\ l^{-1}$). Green symbols indicate stations where an increase of 12 $\mu g\ l^{-1}$ greater than the profile minimum was observed.

Figure 2. Thickness of the nepheloid layer (m). Note scale change at 200 m.

Figure 3. Excess particulate matter in the nepheloid layer ($\mu g\ cm^{-2}$). Note scale change at 1000 $\mu g\ cm^{-2}$. See section 2 for calculation.

Figure 4. Map of log of surface EKE based on satellite observations during 2002-06 (modified from Dixon et al., 2011), with transmissometer station locations superimposed and WOCE lines annotated.

Acknowledgements

We thank our students, colleagues and the many technicians on numerous cruises during the last 38 years for their assistance in collecting the transmissometer data presented here. Supportive cooperation was provided by many personnel from Ocean Data Facility at Scripps (especially James Swift), NOAA personnel, and the many chief scientists during the WOCE, JGOFS, CLIVAR Repeat Hydrography, and GO-SHIP programs. Synthesis of these data has been supported by the National Science Foundation (contract OCE 1536565 to Gardner and Richardson), cooperation with CICS-MD, Univ. of Maryland / NCEI, NOAA and support from the Earl F. Cook Professorship (Gardner). We received funding from NSF for SAVE and JGOFS programs, and from ONR for NABE. We thank three anonymous reviewers for their helpful comments.

Appendix A

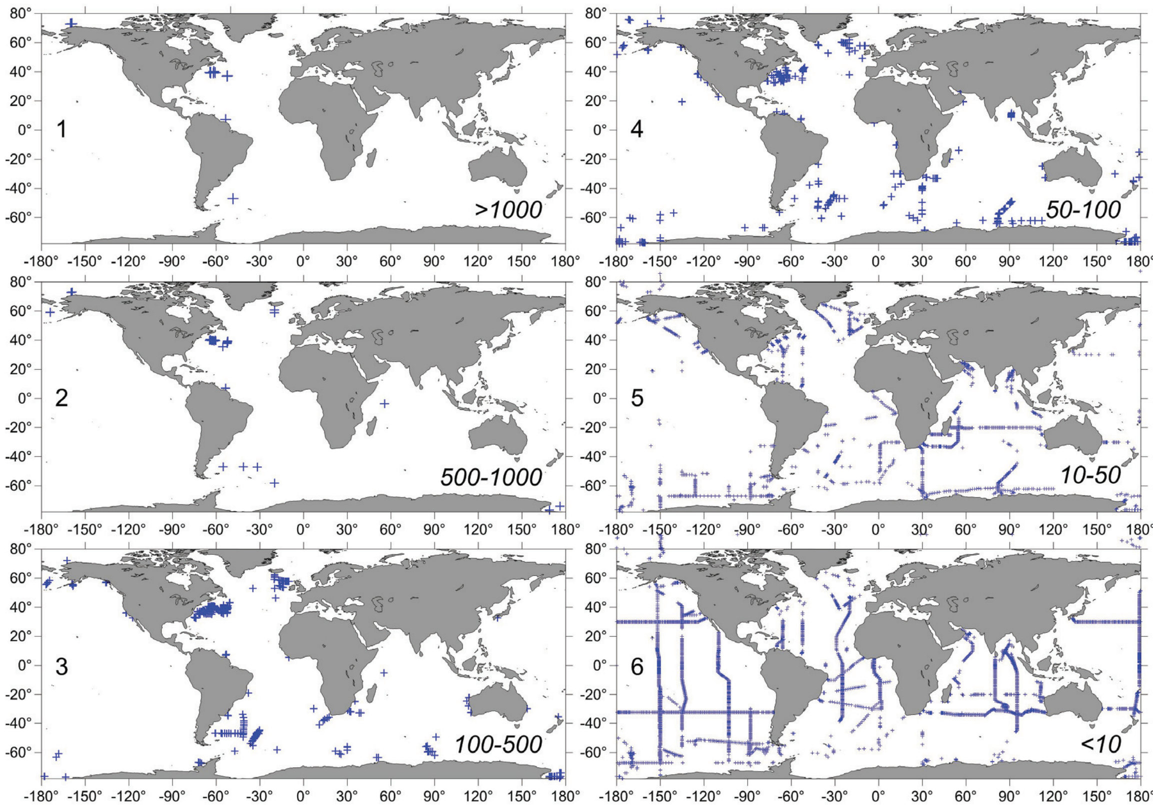

Appendix A. Maps showing stations where PM concentration averaged in the bottom 10 m is 1) >1000 µg l^{-1}, 2) 500-1000 µg l^{-1}, 3) 100-500 µg l^{-1}, 4) 50-100 µg l^{-1}, 5) 10-50 µg l^{-1}, and 6) <10 µg l^{-1} calculated from beam c_p.